Applied Physics Letters ARTICLE pubs.aip.org/aip/apl

Dependent scattering and plasmon coupling in concentrated suspensions of optically hard nanoparticles

Cite as: Appl. Phys. Lett. **125**, 021106 (2024); doi: 10.1063/5.0192977
Submitted: 4 January 2024 · Accepted: 25 June 2024 ·
Published Online: 10 July 2024

Abhinav Bhanawat,[1] Ricardo Martinez,[1] Refet Ali Yalcin,[1,2] Thomas Lee,[1] and Laurent Pilon[1,a)]

AFFILIATIONS

[1]Mechanical and Aerospace Engineering Department, Henry Samueli School of Engineering and Applied Science, University of California, Los Angeles, Los Angeles, California 90095, USA
[2]Saint-Gobain Research Paris, Aubervilliers 93300, France

[a)]**Author to whom correspondence should be addressed:** pilon@seas.ucla.edu. **Tel.:** +1 (310)-206-5598. **Fax:** +1 (310)-206-2302

ABSTRACT

This study establishes the accuracy and efficacy of the recently developed radiative transfer with reciprocal transactions (R^2T^2) method for quickly simulating radiation transfer through concentrated thick suspensions of optically hard nanoparticles featuring a large mismatch in refractive and/or absorption indices compared with their surrounding medium. Concentrated suspensions of optically hard nanoparticles exhibit strong light scattering and dependent scattering effects including both near-field interactions among particles and interferences of scattered waves in the far-field. Concentrated suspensions of metallic nanoparticles also exhibit plasmon coupling effect that leads to widening of absorption peak and red-shift in the peak surface plasmon resonance wavelength. However, predicting these complex interactions between EM waves and particles in thick and concentrated suspensions by explicitly solving Maxwell's equations is computationally intensive, if not impossible. Conventional solutions like Lorenz–Mie theory combined with independent scattering approximation do not account for dependent scattering and plasmon coupling. Furthermore, the dense medium radiative transfer theory is a far-field approximation that does not account for near-field effects, leading to significant errors in predictions, as illustrated in this study. By contrast, the R^2T^2 method's predictions showed excellent agreement with the solutions of Maxwell's equations obtained using the superposition T-matrix method for thin films containing optically hard particles. The method also rigorously accounted for multiple scattering as well as plasmon coupling in thick concentrated suspensions. These results could facilitate the design of plasmonic suspensions used in various energy and environmental applications.

Optically hard nanoparticles refer to a class of nanoparticles that strongly scatter incident light owing to their large relative refractive index m defined as the ratio of the complex index of refraction of the particles $m_p = n_p + ik_p$ and that of the surrounding medium n_m, i.e., $m = m_p/n_m$ at wavelength λ.[1] They are highly coveted in fields such as optical sensing, solar thermal energy conversion, and photoelectrochemistry.[2–4] Notably, optical hardness can be achieved with particles with high refractive index n_p, such as semiconductor particles, and/or with high absorption index k_p, such as metallic particles. For example, semiconductor nanoparticles made of metal oxides such as Cu_2O (Ref. 5) and TiO_2 (Ref. 6) are used to drive photocatalytic reactions for solar water splitting and CO_2 reduction. Likewise, nanofluids containing Ag, Au, Cu, or Si nanoparticles dramatically enhance light absorption in solar water collectors.[7]

Metallic nanoparticles may also exhibit localized surface plasmon resonance (LSPR) resulting in absorption peaks at specific wavelengths depending on their composition and size parameter $\chi = 2\pi r/\lambda$, where r is the particle radius.[8] For example, suspensions of Au nanoparticles exhibit colors ranging from yellow to red depending on the particle size and/or volume fraction.[9,10] Metal nanoparticles are also used to enhance light trapping in solar cells[3] and to design colored radiative cooling coatings.[11]

In all the aforementioned applications, light scattering by nanoparticles may also be affected by the presence and proximity of other nanoparticles, especially when the suspensions are concentrated. This phenomenon is referred to as dependent scattering. It includes near-field interactions among nearest particles and interferences of scattered waves in the far-field,[12] which can result in unexpectedly high transmittance of concentrated colloidal suspensions and paints.[13,14] Additionally, highly absorbing optically hard nanoparticles may exhibit plasmonic coupling among adjacent particles when the

suspension is concentrated.[15] This causes a redshift in the resonance frequency of the nanoparticles that may change the suspensions' appearance and their radiation characteristics.[8] Therefore, accurate prediction of radiation transfer through concentrated suspensions of plasmonic nanoparticles is crucial for a wide range of applications, including photothermal therapy,[16] photovoltaics,[17] as well as plasmonic sensing.[18]

Conventionally, simulation methods solving the 1D radiative transfer equation (RTE) have been used to predict the reflectance and transmittance of nanoparticle suspensions.[19–21] These methods utilize a combination of Lorenz–Mie theory and superposition principle using independent scattering approximation to compute the scattering and absorption coefficients and the scattering phase function of suspensions.[22] To incorporate the effect of far-field interferences, the dense medium radiative transfer theory (DMRT) modifies the scattering coefficient σ_s and the asymmetry parameter g computed by Lorenz–Mie theory using the so-called static structure factor correction.[23] However, both these methods do not account for near-field effects and higher order multiple scattering effects among particles in concentrated suspensions.[14]

Light transfer through a concentrated suspension of optically hard nanoparticles can be simulated accurately by solving Maxwell's equations using the FDTD method, for example, Ref. 24. In this study, Maxwell's equations were solved by utilizing the open-source code CELES[25] that uses superposition T-matrix method on GPUs. It simulates the interactions between a Gaussian beam and a plane-parallel slab containing randomly distributed monodisperse particles. The beam's shape necessitated simulating a cylindrical particle suspension of thickness L and radius R_c.[14] Specifically, particles were initially placed within a rectangular prism of dimensions $4R_c \times 4R_c \times 2L$, from which a cylinder of thickness L and radius R_c was subsequently extracted to mitigate edge effects.[14] The choice of R_c was critical to approximating the suspension as plane-parallel and minimizing photon bundles escaping from the cylinder's sides, with $R_c = 4L$ satisfying these criteria according to preliminary simulations.[14] The superposition T-matrix method is a conceptually exact solution of Maxwell's equations and does not include any assumptions to make the solution simpler, e.g., Born approximation. However, in practice, the accuracy of calculation of T-matrices depends on the maximum degree of spherical harmonics $l_{\max}$ used in the series expansion that describes the scattering properties of particles,[25] as illustrated in Fig. S1 in the supplementary material. Here, $l_{\max} = 3$ was sufficient to achieve numerical convergence. Moreover, it must be noted that unlike the FDTD method, the CELES code does not explicitly compute the near-field at each point but calculates the impact of near-field interactions on the far-field, i.e., overall radiation transfer through the suspensions. Additionally CELES does not solve the radiative transfer equation (RTE) and, therefore, does not require the intermediate steps of computing the scattering and absorption coefficients of the suspensions. However, the method requires large computational resources and is limited to suspension thickness on the same order of magnitude as the wavelength of interest.[14]

To address this issue, researchers have tried using the T-matrix method to compute the scattered electric field and estimate the radiation characteristics of an ensemble of particles and use that as an input into an RTE solver to predict the reflectance, transmittance, and absorptance of a thick medium.[26–28] However, their predictions significantly overestimated the reflectance. This was due to the fact that the T-matrix method simulates a normally incident plane wave from the free space to the particulate medium, whereas in reality, in a thick suspension, most particles encounter a wave scattered from other particles in the particulate medium. Therefore, the T-matrix method includes a coherent scattering component (corresponding to specular reflection at the free space/medium interface) to the computed T-matrix for each ensemble, which leads to overestimation of the scattering coefficient, and subsequently, the reflectance.

Recently, Muinonen *et al.*[29] and Väisänen *et al.*[30] developed the so-called radiative transfer with reciprocal transactions (R^2T^2) method for simulating radiation transfer in semi-infinite heterogeneous dense random media involving multiple scattering. Yalcin *et al.*[14] modified the R^2T^2 framework to predict the normal-hemispherical reflectance and transmittance of thick and concentrated plane-parallel slabs while rigorously accounting for dependent scattering effects. The R^2T^2 method circumvents the overestimation of scattering coefficient by computing the incoherent component of T-matrix by subtracting the coherent component of T-matrix from the free-space total T-matrix. These incoherent components are used to calculate the scattering and absorption coefficients for particle ensembles, which are then used to solve the RTE using the Monte Carlo method. The method involves three steps. Step 1: a large number (~300–900) of spherical particle ensembles of radius R_e ranging from $5r$ to $10r$ containing monodisperse nanoparticles of radius r with the same particle volume fraction as the ergodic medium are generated. Step 2: the open-source fast superposition T-matrix method (FaSTMM)[31] is used for calculating the scattered electric field from an ensemble of particles exposed to a plane-parallel wave. It accounts for near-field interactions, including surface plasmon resonance and plasmonic coupling among adjacent particles and predicts their impact on the far-field. The resolution of the near-field interactions accounted for by the FaSTMM method depends also on the maximum degree of spherical harmonics $l_{\max}$ used in the series expansion describing the scattering properties of particles.[31] The total scattered electric field vector $\boldsymbol{E}_i^{sca}$ for the i^{th} ensemble can be written as[30]

$$\boldsymbol{E}_i^{sca} = \sum_{v=1}^{N_0} \sum_{w=-v}^{v} \left(a_{wv1,i}\boldsymbol{M}_{wv} + a_{wv2,i}\boldsymbol{N}_{wv}\right), \tag{1}$$

where $a_{wv1,i}$ and $a_{wv2,i}$ are the spherical vector wave function coefficients corresponding to polarizations 1 and 2, while $\boldsymbol{M}_{wv}$ and $\boldsymbol{N}_{wv}$ are the base vectors comprising of vector spherical wave functions. The integer N_0 represents the degree of expansion needed for convergence.[30] The total scattering $C_{sca,i}$ and extinction $C_{ext,i}$ cross sections of the ensemble are respectively expressed as[30]

$$C_{sca,i} = \frac{1}{q^2} \sum_{v=1}^{N_0} \sum_{w=-v}^{v} \left(|a_{wv1,i}|^2 + |a_{wv2,i}|^2\right) \tag{2}$$

and

$$C_{ext,i} = \frac{1}{q^2} \sum_{v=1}^{N_0} \sum_{w=-v}^{v} Re(a_{wv1,i} + a_{wv2,i}), \tag{3}$$

where $q = 2\pi/\lambda$ is the angular wavenumber. The absorption cross section of particle ensemble "i" is given by $C_{abs,i} = C_{ext,i} - C_{sca,i}$. The T-matrix $\boldsymbol{T}_i$ for the i^{th} ensemble can be computed from the relation[30]

$$\begin{pmatrix} a_{wv1,i} \\ a_{wv2,i} \end{pmatrix} = \boldsymbol{T}_i \begin{pmatrix} f_{wv1} \\ f_{wv2} \end{pmatrix}, \tag{4}$$

where f_{wv1} and f_{wv2} are the coefficients of the incident electric field vector $\boldsymbol{E}^{inc}$. This T-matrix $\boldsymbol{T}_i$ can also be expressed as the sum of its incoherent $\boldsymbol{T}_i^{ic}$ and coherent $\boldsymbol{T}^c$ components, the latter being identical for all ensembles and computed in an analogous manner to $\boldsymbol{T}_i$ but using the coefficients of the coherent scattered electric field written as[30]

$$\boldsymbol{E}^{sca,c} = \lim_{N\to\infty} \frac{1}{N} \sum_{i=1}^{N} \boldsymbol{E}_i^{sca}. \tag{5}$$

Then, the incoherent component $\boldsymbol{T}_i^{ic}$ can be calculated using $\boldsymbol{T}_i^{ic} = \boldsymbol{T}_i - \boldsymbol{T}^c$. The corresponding coefficients of the incoherent scattered electric field $a_{wv1,i}^{ic}$ and $a_{wv2,i}^{ic}$ are given by[30]

$$\begin{pmatrix} a_{wv1,i}^{ic} \\ a_{wv2,i}^{ic} \end{pmatrix} = \boldsymbol{T}_i^{ic} \begin{pmatrix} f_{wv1} \\ f_{wv2} \end{pmatrix}. \tag{6}$$

Then, the incoherent scattering cross section of the i^{th} ensemble can be defined as[30]

$$C_{sca,i}^{ic} = \frac{1}{q^2} \sum_{v=1}^{N_0} \sum_{w=-v}^{v} \left(|a_{wv1,i}^{ic}|^2 + |a_{wv2,i}^{ic}|^2 \right). \tag{7}$$

Similarly, the incoherent extinction coefficient β_i^{ic} and the incoherent scattering albedo ω_i^{ic} of the i^{th} ensemble are, respectively, expressed as[30]

$$\beta_i^{ic} = \frac{C_{sca,i}^{ic} + C_{abs,i}}{V_{e,i}} \quad \text{and} \quad \omega_i^{ic} = \frac{C_{sca,i}^{ic}}{C_{sca,i}^{ic} + C_{abs,i}}, \tag{8}$$

where $V_{e,i}$ is the volume of the particle ensemble. The incoherent scattering and absorption coefficients of the i^{th} ensemble are, respectively, defined as[30]

$$\sigma_{s,i}^{ic} = \beta_i^{ic} \omega_i^{ic} \quad \text{and} \quad \kappa_i = \beta_i^{ic} \left(1 - \omega_i^{ic}\right). \tag{9}$$

Finally, these coefficients are averaged over all ensembles to obtain the radiation characteristics of the suspension. Step 3: the radiative transfer equation (RTE) is solved via the Monte Carlo method. A wave-tracing approach is used where the scattered radiation from the previous ensemble, computed using radiation characteristics of a randomly

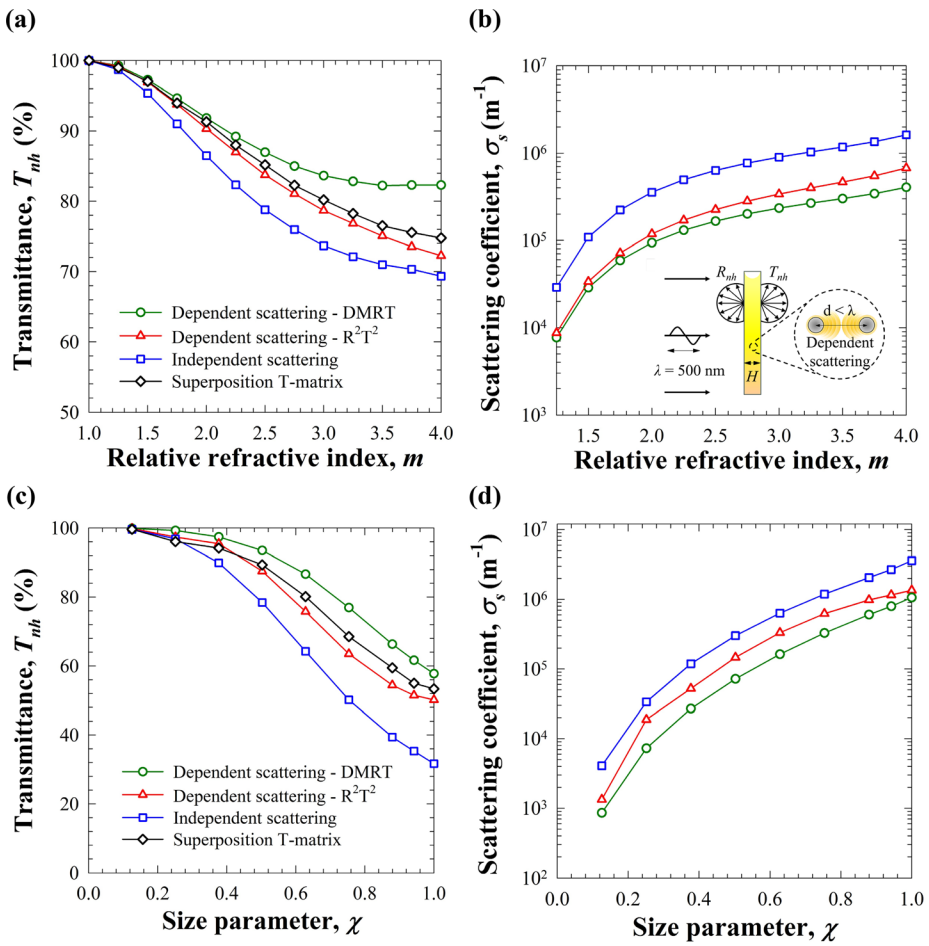

FIG. 1. Comparison of (a,c) the normal-hemispherical transmittance T_{nh} and (b,d) the scattering coefficient σ_s of a film of thickness $H = 2\,\mu$m containing non-absorbing particles as functions of (a,b) relative refractive index $m = n_p/n_m$ ($k_p = k_m = 0$) or (c,d) particle size parameter χ predicted by solving the RTE using the three models of interest. For (a,b), the particles had radius $r = 50$ nm and volume fraction $f_v = 10\%$, whereas for (c,d), the particles had a relative refractive index $m = 2.5$ and $f_v = 20\%$. The predictions by the superposition T-matrix method are used as references in (a,c). In all cases, $R_{nh} = 1 - T_{nh}$.

sampled ensemble, is used as incident radiation for the next ensemble, thereby accounting for the non-planar nature of the radiation incident on most particle ensembles inside the medium.[14,30] The ensemble-averaged extinction coefficient is used to determine the pathlength for wave-tracing.

Predictions of the R^2T^2 method showed excellent agreement with those from the superposition T-matrix method for concentrated suspensions of silica nanoparticles of radius r varying from 15 to 35 nm, volume fraction up to 40%, and suspension thickness up to 5 μm.[14] The model was also validated against measurements of spectral normal-hemispherical reflectance and transmittance of (i) silica nanoparticle suspensions containing particles with radius r around 8–14 nm and volume fraction $f_v \leq 15\%$[14] and (ii) nanoemulsions with oil droplet radius around 10 nm and volume fraction $f_v \leq 20\%$.[32] The model accurately predicted an increase in transmittance with increasing particle volume fraction owing to dependent scattering. By contrast, the DMRT method overpredicted the transmittance, whereas assuming independent scattering significantly underestimated the transmittance at large volume fractions. Overall, the R^2T^2 method could adequately simulate dependent scattering effects in thick colloidal suspensions of non-absorbing optically soft nanoparticles. However, its validity and accuracy for optically hard nanoparticles has not been established.

This study aims to identify the most appropriate and accurate method to simulate radiation transfer through concentrated and thick suspensions of optically hard nanoparticles exhibiting multiple scattering and/or plasmonic effects over wide ranges of relative complex index of refraction m, particle size parameter χ, and suspension thickness H. In all cases, we solved the RTE using different simulation methods to predict the normal-hemispherical reflectance R_{nh} and transmittance T_{nh} of the suspensions using either (i) independent scattering approximation or accounting for dependent scattering using (ii) the DMRT or (iii) the R^2T^2 method. For thin films, the results were compared with the predictions by the superposition T-matrix method. In all cases, the nanoparticles were monodisperse and randomly distributed in a non-absorbing continuous medium of refractive index $n_m = 1.0$ at wavelength $\lambda = 500$ nm, unless stated otherwise. Additionally, the surrounding medium was non-absorbing and had a refractive index $n_{sur} = 1.0$ such that boundary reflection at the continuous medium/surrounding interfaces could be ignored.

Figure 1(a) compares the normal-hemispherical transmittance T_{nh} of a film of thickness $H = 2$ μm containing non-absorbing nanoparticles ($k_p = 0$) as a function of relative refractive index $m = n_p/n_m$ predicted by solving the RTE using the three models of interest with the predictions by the superposition T-matrix method. The nanoparticles had radius $r = 50$ nm and volume fraction $f_v = 10\%$. In the absence of absorption, the reflectance R_{nh} was such that $R_{nh} = 1 - T_{nh}$. Figure 1(a) establishes that assuming independent scattering significantly underestimated the transmittance over the range of relative refractive index considered. By contrast, predictions by the DMRT method were in good agreement with the predictions by the superposition T-matrix method only for relative refractive index $m \leq 2$ but deviated substantially beyond. Finally, predictions by the R^2T^2 method fell within 3% of the predictions by the superposition T-matrix method for all relative refractive index m considered.

Figure 1(b) plots the corresponding scattering coefficient σ_s as a function of m predicted by the three models considered. As expected, in all cases, the scattering coefficients increased with increasing index mismatch. However, the increase in σ_s predicted by the DMRT method was more subdued in comparison to that predicted by the R^2T^2 method because the DMRT method could not account for higher order scattering terms for large relative refractive index m. Finally, the scattering coefficient σ_s predicted by assuming independent scattering was significantly larger than those predicted by the DMRT and R^2T^2 methods for all values of m considered. This resulted in overestimation of the reflectance and underestimation of the transmittance [Fig. 1(a)].

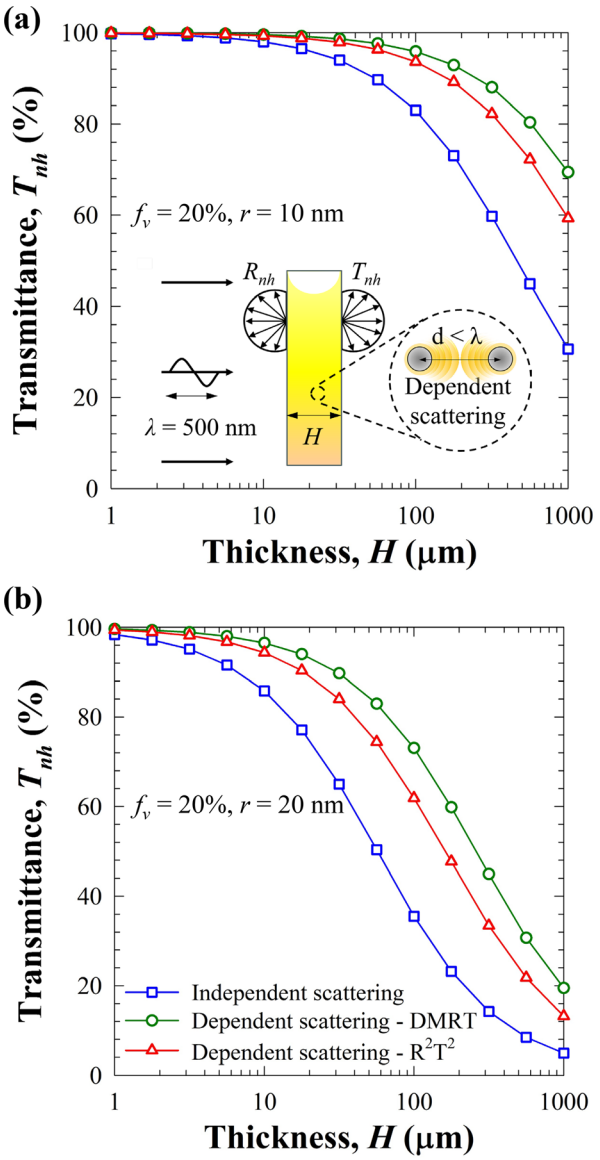

FIG. 2. Comparison of the normal-hemispherical transmittance T_{nh} of a suspension containing non-absorbing nanoparticles of radii (a) $r = 10$ nm and (b) $r = 20$ nm as a function of suspension thickness H predicted by solving the RTE using the three models of interest. Particles had a relative refractive index $m = 2.5$ and volume fraction $f_v = 20\%$. In all cases, $R_{nh} = 1 - T_{nh}$.

Figure 1(c) compares the normal-hemispherical transmittance T_{nh} of a film of thickness $H = 2\,\mu$m containing non-absorbing nanoparticles as a function of particle size parameter χ predicted by solving the RTE using the three models of interest with the predictions by the superposition T-matrix method. The particles were optically hard with relative refractive index $m = 2.5$ and volume fraction $f_v = 20\%$. Figure 1(c) indicates that assuming independent scattering consistently underestimated the transmittance T_{nh}, while the DMRT method overestimated it as compared to the predictions by the superposition T-matrix method. Finally, predictions by the R^2T^2 method showed good agreement with the predictions by the superposition T-matrix method for all size parameters χ considered.

Figure 1(d) plots the corresponding scattering coefficient σ_s as a function of particle size parameter χ predicted by the three models of interest. As expected, the scattering coefficients increased significantly with increasing size parameter χ. Here again, assuming independent scattering overestimated the scattering coefficient σ_s compared with that predicted by the R^2T^2 method, while the DMRT method underpredicted it.

Overall, these observations were consistent with the previously reported results for suspensions of optically soft particles[14] and expand the range of applicability of the R^2T^2 method.

Figure 2 compares the normal-hemispherical transmittance T_{nh} at wavelength $\lambda = 500$ nm of colloidal suspensions with nanoparticles of refractive index $n_p = 2.5$ and volume fraction $f_v = 20\%$ for particle radius (a) $r = 10$ nm and (b) $r = 20$ nm predicted as functions of suspension thickness H by solving the RTE using the three models of interest. Figure 2 shows that the transmittance decreased with increasing suspension thickness H due to multiple scattering. Here again, assuming independent scattering consistently underestimated the transmittance compared to when dependent scattering was accounted for. Furthermore, the difference between predictions by the R^2T^2 method and the DMRT method grew more pronounced as the suspension thickness H increased, highlighting the cumulative impact of multiple scattering in thicker suspensions. These results can be crucial in designing metamaterials using non-absorbing nanoparticles for radiative cooling, optical sensing, and anti-reflective applications.[33–35]

Figure 3 compares the spectral normal-hemispherical (a,c) transmittance $T_{nh,\lambda}$, (b) absorptance $A_{n,\lambda}$, and (d) reflectance $R_{nh,\lambda}$ from 300 to 500 nm predicted by solving the RTE using the three models of interest with the predictions by the superposition T-matrix method for films of thickness $H = 0.5\,\mu$m containing Ag nanoparticles with radius $r = 10$ nm and volume fraction (a,b) $f_v = 1\%$ or (c,d) $f_v = 20\%$. The spectral refractive $n_{p,\lambda}$ and absorption $k_{p,\lambda}$ indices of Ag nanoparticles

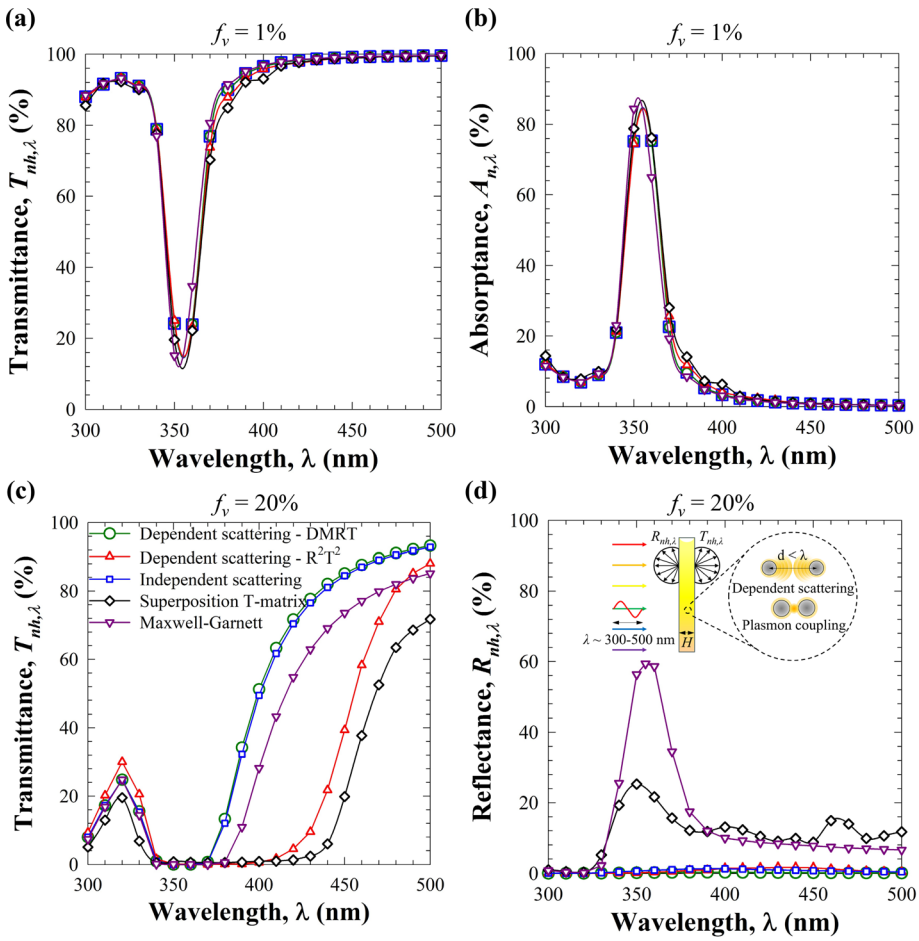

FIG. 3. Comparison of the spectral normal-hemispherical (a,c) transmittance $T_{nh,\lambda}$, (b) absorptance $A_{n,\lambda}$, and (d) reflectance $R_{nh,\lambda}$ of a thin film of thickness $H = 0.5\,\mu$m containing Ag nanoparticles of radius $r = 10$ nm as functions of wavelength λ predicted by solving the RTE using the three models of interest for particle volume fractions (a,b) $f_v = 1\%$ and (c,d) $f_v = 20\%$. The spectral predictions by the superposition T-matrix method and those obtained using Maxwell–Garnett model are used as references.

were obtained from Ref. 36. Predictions for the film approximated as homogeneous with effective refractive and absorption indices given by Maxwell–Garnett effective medium approximation (EMA) are also provided as references in Figs. 3(a)–3(d). Figures 3(a) and 3(b) show that the spectral predictions obtained by solving the RTE using the three models of interest, as well as those predicted using the EMA were in excellent agreement with the predictions by the superposition T-matrix method for particle volume fraction $f_v = 1\%$ at all wavelengths considered. All four models predicted a significant decrease in transmittance $T_{nh,\lambda}$ and a peak in absorptance $A_{n,\lambda}$ around $\lambda \sim 355$ nm resulting from surface plasmon resonance exhibited by individual Ag nanoparticles. The reflectance $R_{nh,\lambda}$ was negligible for all wavelengths because the suspension was dilute and the nanoparticles were widely dispersed in a thin film of thickness 0.5 μm, resulting in minimal scattering. By contrast, Figs. 3(c) and 3(d) indicate that as f_v increased to 20%, predictions by the DMRT method as well as those obtained by assuming independent scattering deviated significantly from the predictions by the superposition T-matrix method. This was because both methods could not account for the coupling of surface plasmons taking place among Ag nanoparticles at large volume fractions. By contrast, the trends in the predictions by the R^2T^2 method were similar to those by the superposition T-matrix method. The R^2T^2 method was able to account for plasmon coupling effects via the fast superposition T-matrix method (FaSTMM)[31] that led to significant widening of the absorption band between 350 and 450 nm and the red-shift in $T_{nh,\lambda}$ for large volume fractions [Fig. 3(c)]. The difference between predictions by the R^2T^2 method and the predictions by the superposition T-matrix method can be attributed to the fact that the R^2T^2 method does not account for coherent backscattering from the surrounding/film interface but only considers absorption and incoherent scattering from the bulk of the film.[14] At large particle volume fractions, the film containing Ag nanoparticles behaves as a refractive and reflective medium, which contributes to the reflectance via coherent (specular) scattering from the top and bottom boundaries of the film. This is confirmed by the large reflectance $R_{nh,\lambda}$ predicted for the homogeneous slabs with effective optical properties given by Maxwell–Garnett model for $f_v = 20\%$. Since the R^2T^2 method does not account for coherent scattering, it underestimated the reflectance of concentrated suspensions of plasmonic nanoparticles such as Ag, as illustrated in Fig. 3(d). Note that the independent scattering approximation and the DMRT methods did not account either for specular reflection at the free space/medium interface since the host medium and its surroundings were chosen to be of the same material, namely air. Nevertheless, predictions of transmittance $T_{nh,\lambda}$ by the R^2T^2 method

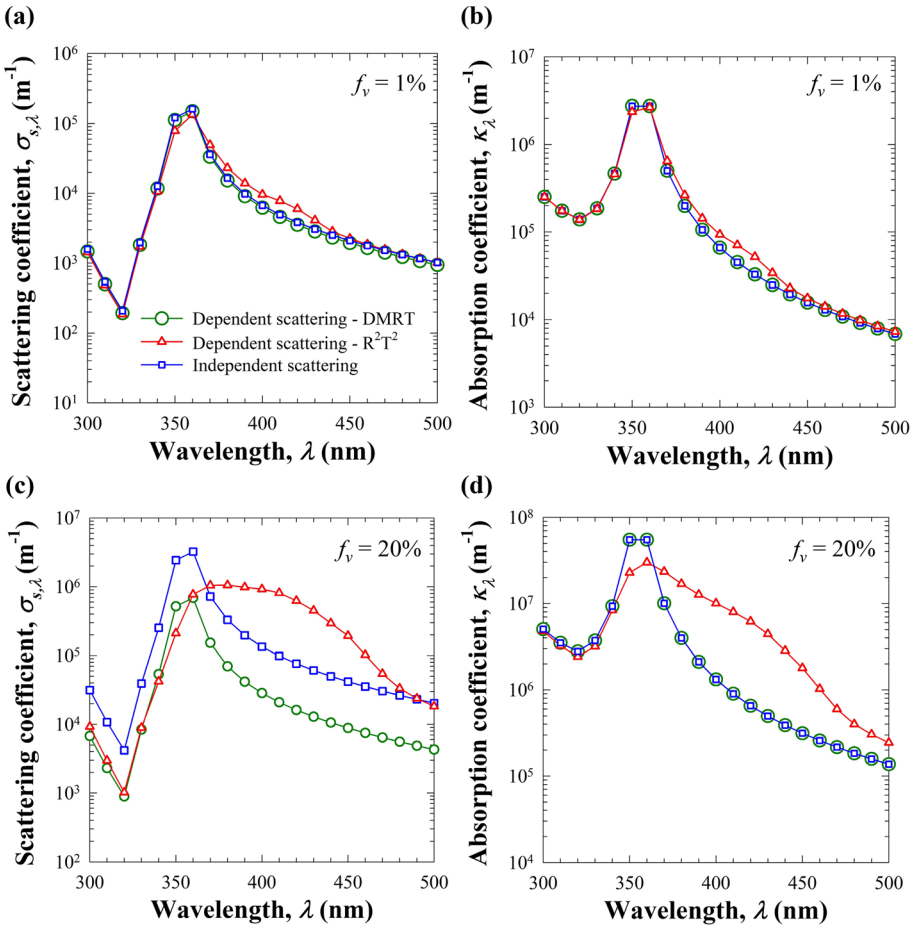

FIG. 4. Comparison of the spectral (a,c) scattering $\sigma_{s,\lambda}$ and (b,d) absorption κ_λ coefficients corresponding to the data plotted in Fig. 3.

aligned more closely with the trends of the predictions by the superposition T-matrix method as compared to those by the independent scattering approximation and the DMRT method.

Figure 4 compares the spectral (a,c) scattering $\sigma_{s,\lambda}$ and (b,d) absorption κ_λ coefficients predicted using the three models of interest corresponding to data plotted in Fig. 3. Figure 4 shows that the predictions by all three models agreed with each other for small volume fraction $f_v = 1\%$. All models predicted peaks in the scattering and absorption coefficients around $\lambda = 355$ nm owing to surface plasmon resonance in Ag nanoparticles. As expected, all three models predicted an increase in the scattering and absorption coefficients as the volume fraction increased to $f_v = 20\%$. However, the DMRT method predicted a smaller spectral scattering coefficient compared to that predicted using the independent scattering approximation, while the spectral absorption coefficient was the same for both models. This can be attributed to the fact that the static structure factor used in DMRT method to account for dependent scattering effects only modifies the scattering cross section of particles, while the absorption cross section remains the same as that predicted based on Lorenz–Mie theory. Notably, both these models predicted the same peak resonance wavelength for volume fractions $f_v = 1\%$ as well as for $f_v = 20\%$. This establishes that these two models cannot account for plasmon coupling effects among adjacent particles. On the other hand, the R^2T^2 method rigorously accounted for plasmon coupling effects by predicting widening of the peaks in the scattering and absorption coefficients and also a red-shift in the peak resonance wavelength as the volume fraction increased from 1% to 20%.

Figure 5 compares (a) the normal-hemispherical reflectance R_{nh} and (b) the normal absorptance A_n of a suspension ($n_m = 1.0$) of thickness $H = 1$ mm containing Ag nanoparticles of radius $r = 50$ nm as functions of particle volume fraction f_v predicted by solving the RTE using the three models of interest at wavelength $\lambda = 400$ nm. The corresponding scattering σ_s and absorption κ coefficients are presented in Figs. 5(c) and 5(d), respectively. Interestingly, Fig. 5(a) shows that the reflectance R_{nh} predicted by assuming independent scattering remained nearly constant for volume fraction $f_v \geq 0.01\%$, despite an increase in the scattering σ_s and absorption κ coefficients observed in Figs. 5(c) and 5(d). This can be attributed to the large optical thickness ($\sim$12) of thick suspensions of Ag nanoparticles with $f_v = 0.01\%$ and $H = 1$ mm that causes the suspensions to effectively behave as semi-infinite. Indeed, the reflectance R_{nh} predicted by assuming independent scattering plateaued for optical thickness exceeding 10 (see Fig. S3 in the supplementary material). Predictions by the DMRT method and by the R^2T^2 method agreed with those obtained by assuming independent scattering for $f_v < 1\%$. However, for larger f_v, the dependent scattering effects significantly decreased the reflectance R_{nh} and allowed

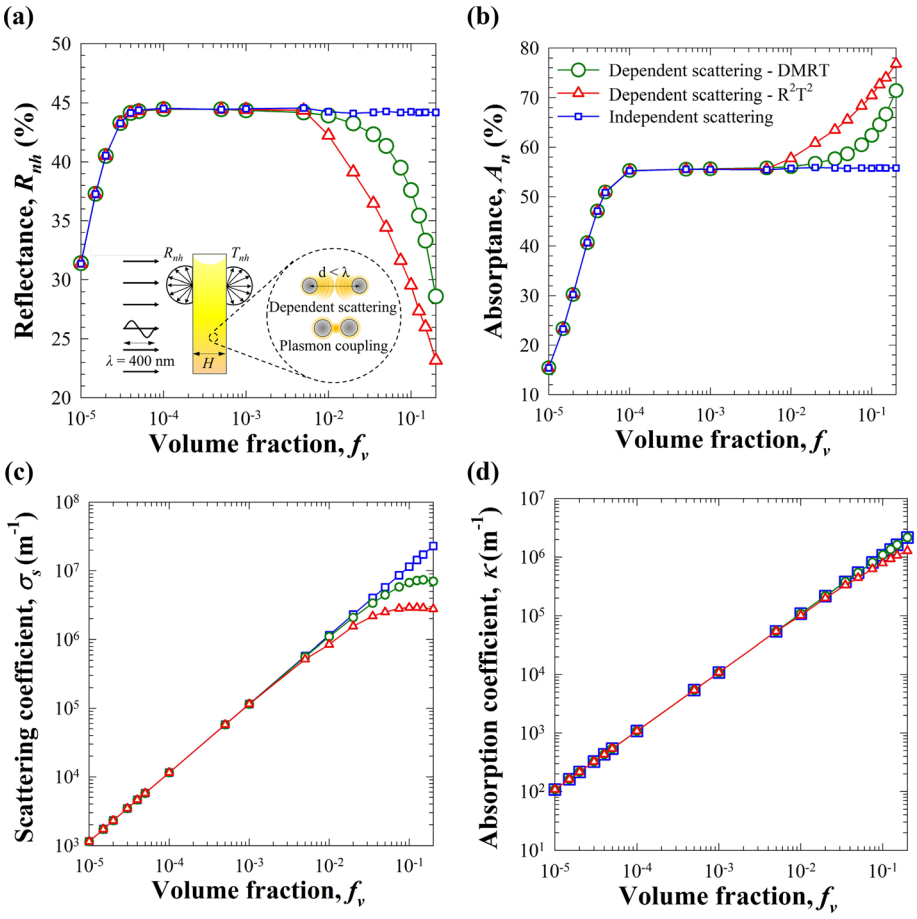

FIG. 5. Comparison of (a) the normal-hemispherical reflectance R_{nh}, (b) the normal absorptance A_n, (c) the scattering coefficient σ_s, and (d) the absorption coefficient κ of a 1 mm thick suspension containing Ag nanoparticles of radius $r = 50$ nm as functions of volume fraction f_v predicted by solving the RTE using the three models of interest at wavelength $\lambda = 400$ nm.

more radiation to penetrate inside the medium and get absorbed. Additionally, the difference in the predictions of reflectance R_{nh} by the DMRT method and by the R^2T^2 method increased substantially as the volume fraction increased due to the difference in the predicted scattering coefficients σ_s [Fig. 5(c)]. Finally, Fig. 5(d) shows that the absorption coefficients κ predicted by the DMRT method and by the independent scattering approximation were identical. However, these two models overestimated κ compared to the R^2T^2 method as the volume fraction increased. This can be attributed to plasmon coupling effects in concentrated suspensions of Ag nanoparticles that were accounted for by the R^2T^2 method but ignored by the DMRT method and the independent scattering approximation.

Overall, this study established that dependent scattering, and plasmon coupling prevailed in concentrated colloidal suspensions of optically hard nanoparticles and influenced significantly their interaction with incident EM waves. These phenomena had a substantial cumulative effect on the reflectance, transmittance, and/or absorptance of colloidal suspensions, especially for large suspension thickness. The R^2T^2 method was found to be the most suitable and accurate to simulate these dependent effects in concentrated and thick suspensions when solving Maxwell's equations becomes computationally impractical or impossible. The R^2T^2 method accounted for near-field effects such as plasmon coupling among particles and predicted their impact on the far-field, unlike the DMRT method and the independent scattering approximation. Therefore, the R^2T^2 method should be preferred for its minimal computational resource requirements and high accuracy over a wide range of particle relative complex index of refraction, size parameter, volume fraction, and suspension thickness.

See the supplementary material for Fig. S1, which compares the spectral (a) normal-hemispherical transmittance $T_{nh,\lambda}$ and (b) absorptance $A_{n,\lambda}$ of a thin film of thickness $H = 0.5\ \mu$m and refractive index $n_m = 1.0$ containing Ag nanoparticles of radius $r = 10$ nm and volume fraction $f_v = 5\%$ predicted by CELES[25] as functions of wavelength λ for different values of l_{max}, i.e., the maximum degree of spherical harmonics used in the series expansion that describes the scattering properties of particles. Here, numerical convergence was achieved for $l_{max} = 3$. Figure S2 plots the normal-hemispherical transmittance T_{nh} of a film of thickness $H = 2\ \mu$m containing non-absorbing nanoparticles ($k_p = 0$) as a function of relative refractive index $m = n_p/n_m$ predicted by solving the RTE using the R^2T^2 method. The particles were either monodisperse with radius $r = 50$ nm or polydisperse with mean radius $\bar{r} = 50$ nm and standard deviation $\sigma = 5$ nm or 10 nm and had volume fraction $f_v = 10\%$. Figure S2 shows that the transmittance predictions for polydisperse particle size distributions were within 10% of those for the monodisperse size distribution. Figure S3 shows that (a) the normal-hemispherical reflectance R_{nh} and (b) the normal absorptance A_n of 1 mm thick suspensions containing monodisperse and randomly distributed Ag or Al nanoparticles of radius $r = 30$ or 50 nm predicted by solving the RTE using the independent scattering approximation plateaued as the optical thickness βH increased.

This study was supported, in part, by the National Science Foundation NRT-INFEWS: Integrated Urban Solutions for Food, Energy, and Water Management (Grant No. DGE-1735325). This work used computational and storage services associated with the Hoffman2 Shared Cluster provided by UCLA Institute for Digital Research and Education's Research Technology Group. Abhinav Bhanawat is grateful to the UCLA Mechanical and Aerospace Engineering Department for financial support through a graduate research fellowship. The authors are grateful to Dr. Amos Egel and Dr. Johannes Markkanen for help with the CELES and FaSTMM methods.

AUTHOR DECLARATIONS

Conflict of Interest

The authors have no conflicts to disclose.

Author Contributions

Abhinav Bhanawat: Formal analysis (lead); Investigation (lead); Methodology (lead); Software (equal); Validation (equal); Visualization (lead); Writing – original draft (lead); Writing – review & editing (equal). **Ricardo Martinez:** Methodology (equal); Software (equal). **Refet Ali Yalcin:** Conceptualization (lead); Methodology (equal); Software (equal); Validation (equal). **Thomas Lee:** Methodology (equal); Software (equal). **Laurent Pilon:** Conceptualization (equal); Funding acquisition (lead); Supervision (lead); Writing – review & editing (equal).

DATA AVAILABILITY

The data that support the findings of this study are available within the article and its supplementary material.

REFERENCES

[1]S. K. Sharma and D. J. Sommerford, *Light Scattering by Optically Soft Particles: Theory and Applications* (Springer Science & Business Media, Berlin, Germany, 2006).
[2]M. Li, S. K. Cushing, and N. Wu, "Plasmon-enhanced optical sensors: A review," Analyst **140**(2), 386–406 (2015).
[3]H. A. Atwater and A. Polman, "Plasmonics for improved photovoltaic devices," Nat. Mater. **9**(3), 205–213 (2010).
[4]P. Subramanyam, B. Meena, V. Biju, H. Misawa, and S. Challapalli, "Emerging materials for plasmon-assisted photoelectrochemical water splitting," J. Photochem. Photobiol., C **51**, 100472 (2022).
[5]M. Tariq, M. D. Koch, J. W. Andrews, and K. E. Knowles, "Correlation between surface chemistry and optical properties in colloidal Cu_2O nanoparticles," J. Phys. Chem. C **124**(8), pp. 4810–4819 (2020).
[6]Q. Wang and K. Domen, "Particulate photocatalysts for light-driven water splitting: Mechanisms, challenges, and design strategies," Chem. Rev. **120**(2), 919–985 (2019).
[7]P. Nagarajan, J. Subramani, S. Suyambazhahan, and R. Sathyamurthy, "Nanofluids for solar collector applications: A review," Energy Procedia **61**, 2416–2434 (2014).
[8]Z. M. Zhang, *Nano/Microscale Heat Transfer*, 2nd ed. (Springer Nature, Switzerland, 2020).
[9]T. Ung, L. M. Liz-Marzan, and P. Mulvaney, "Gold nanoparticle thin films," Colloids Surf., A **202**(2–3), 119–126 (2002).
[10]R. Wilson, "The use of gold nanoparticles in diagnostics and detection," Chem. Soc. Rev. **37**(9), 2028–2045 (2008).
[11]R. A. Yalçın, E. Blandre, K. Joulain, and J. Drévillon, "Colored radiative cooling coatings with nanoparticles," ACS Photonics **7**(5), 1312–1322 (2020).
[12]T. Galy, D. Huang, and L. Pilon, "Revisiting independent versus dependent scattering regimes in suspensions or aggregates of spherical particles," J. Quant. Spectrosc. Radiat. Transfer **246**, 106924 (2020).
[13]W. Vargas, P. Greenwood, J. Otterstedt, and G. Niklasson, "Light scattering in pigmented coatings: Experiments and theory," Sol. Energy **68**(6), 553–561 (2000).

[14]R. A. Yalcin, T. Lee, G. N. Kashanchi, J. Markkanen, R. Martinez, S. H. Tolbert, and L. Pilon, "Dependent scattering in thick and concentrated colloidal suspensions," ACS Photonics **9**(10), 3318–3332 (2022).
[15]P. K. Jain, X. Huang, I. H. El Sayed, and M. A. El-Sayed, "Review of some interesting surface plasmon resonance-enhanced properties of noble metal nanoparticles and their applications to biosystems," Plasmonics **2**, 107–118 (2007).
[16]M. Kim, J. H. Lee, and J. M. Nam, "Plasmonic photothermal nanoparticles for biomedical applications," Adv. Sci. **6**(17), 1900471 (2019).
[17]S. Pillai and M. Green, "Plasmonics for photovoltaic applications," Sol. Energy Mater. Sol. Cells **94**(9), 1481–1486 (2010).
[18]J. Boken, P. Khurana, S. Thatai, D. Kumar, and S. Prasad, "Plasmonic nanoparticles and their analytical applications: A review," Appl. Spectrosc. Rev. **52**(9), 774–820 (2017).
[19]M. Abdelrahman, P. Fumeaux, and P. Suter, "Study of solid-gas-suspensions used for direct absorption of concentrated solar radiation," Sol. Energy **22**(1), 45–48 (1979).
[20]F. J. Miller and R. W. Koenigsdorff, "Thermal modeling of a small-particle solar central receiver," J. Sol. Energy Eng. **122**(1), 23–29 (2000).
[21]H. Tyagi, P. Phelan, and R. Prasher, "Predicted efficiency of a low-temperature nanofluid-based direct absorption solar collector," J. Sol. Energy Eng. **131**(4), 041004 (2009).
[22]M. F. Modest and S. Mazumder, *Radiative Heat Transfer*, 4th ed. (Academic Press, New York, 2021).
[23]M. I. Mishchenko, "Asymmetry parameters of the phase function for densely packed scattering grains," J. Quant. Spectrosc. Radiat. Transfer **52**(1), 95–110 (1994).
[24]D. M. Sullivan, *Electromagnetic Simulation Using the FDTD Method* (John Wiley & Sons, Hoboken, NJ, 2013).
[25]A. Egel, L. Pattelli, G. Mazzamuto, D. S. Wiersma, and U. Lemmer, "CELES: CUDA-accelerated simulation of electromagnetic scattering by large ensembles of spheres," J. Quant. Spectrosc. Radiat. Transfer **199**, 103–110 (2017).
[26]S. C. Lee, "Dependent vs independent scattering in fibrous composites containing parallel fibers," J. Thermophys. Heat Transfer **8**(4), 641–646 (1994).
[27]J. Zeng and Y. Xuan, "Analysis on interaction between solar light and suspended nanoparticles in nanofluids," J. Quant. Spectrosc. Radiat. Transfer **269**, 107692 (2021).
[28]Z. Aoyu, W. Fuqiang, D. Yan, Y. Dongling, and X. Weixin, "Dependent scattering criterion modification of disordered dispersed particulate medium with the consideration of particle random distribution and high complex refractive index effects," Int. J. Heat Mass Transfer **197**, 123331 (2022).
[29]K. Muinonen, J. Markkanen, T. Väisänen, J. Peltoniemi, and A. Penttilä, "Multiple scattering of light in discrete random media using incoherent interactions," Opt. Lett. **43**(4), 683–686 (2018).
[30]T. Väisänen, J. Markkanen, A. Penttilä, and K. Muinonen, "Radiative transfer with reciprocal transactions: Numerical method and its implementation," PLoS One **14**(1), e0210155 (2019).
[31]J. Markkanen and A. J. Yuffa, "Fast superposition T-matrix solution for clusters with arbitrarily-shaped constituent particles," J. Quant. Spectrosc. Radiat. Transfer **189**, 181–188 (2017).
[32]R. Martinez, A. Bhanawat, R. A. Yalcin, and L. Pilon, "Rigorous accounting for dependent scattering in thick and concentrated nanoemulsions," J. Phys. Chem. C **128**(15), 6419–6430 (2024).
[33]Z. Huang and X. Ruan, "Nanoparticle embedded double-layer coating for daytime radiative cooling," Int. J. Heat Mass Transfer **104**, 890–896 (2017).
[34]J. Loste, J.-M. Lopez-Cuesta, L. Billon, H. Garay, and M. Save, "Transparent polymer nanocomposites: An overview on their synthesis and advanced properties," Prog. Polym. Sci. **89**, 133–158 (2019).
[35]L. J. Romasanta, L. D'alençon, S. Kirchner, C. Pradère, and J. Leng, "Thin coatings of cerium oxide nanoparticles with anti-reflective properties," Appl. Sci. **9**(18), 3886 (2019).
[36]H. U. Yang, J. D'Archangel, M. L. Sundheimer, E. Tucker, G. D. Boreman, and M. B. Raschke, "Optical dielectric function of silver," Phys. Rev. B **91**(23), 235137 (2015).